

## THE STRUCTURE OF BUBBLY FLOW THROUGH VENTURIS

N. T. THANG

Darling Downs Institute of Advanced Education, Queensland, Australia

and

M. R. DAVIS

University of New South Wales, New South Wales, Australia

(Received 3 August 1977; in revised form 20 June 1978)

**Abstract**—The phase structure of vertical air–water mixture flows through venturis were investigated using area contraction ratios of 3.16 and 7.11 and with variations in angles of convergence and divergence. The flow conditions were predominantly of the bubbly type and covered a range of gas volume fraction at the throat between 0.2 and 0.6 for average mixture velocities of up to 32 m/s. Resistivity probe signals indicating void fluctuations were analyzed to yield local void fraction, bubble velocity, bubble detection rate and probability density function of bubble sizes in the flow. Velocity ratios were also obtained to provide information on the overall behaviour of the two concurrent phases. The resistivity probe was shown to give reliable results for bubble flows in a wide range of speeds indicating velocity ratios up to 1.7 in the venturi throat. All flows tended toward a stable and well-mixed bubbly pattern downstream of the venturi exit following a sufficient length. The void and velocity profiles here always appeared to be characterized by a local maximum in the pipe centre, the local maximum close to the wall of some of the inlet flows being eliminated. Bubble coalescence was noted in the convergent passage whilst significant bubble fragmentation in the divergent passage was observed from the results.

### 1. INTRODUCTION

Studies of gas–liquid flow in nozzles appear to concentrate on critical flow phenomena in high quality flows (Smith *et al.* 1968; Carofano & McManus 1969). The character of lower quality two-component gas–liquid flows, namely bubble or dispersed flows, through the common configuration of a convergent–divergent nozzle appears to have received little attention in the literature and little information is currently available on the structure of such a flow through a venturi-type contraction.

A number of measuring techniques have been devised in recent years to study two-phase flow structure. The earlier techniques developed for void fraction measurement only provided time-average and area-average values. Amongst these the gamma-ray attenuation technique was more commonly used (Petrick 1958; Vogrin 1963). To gain a better understanding of the flow, instruments have been developed to detect local instantaneous phase variations. These instruments and their operating principles can be broadly divided into three groups: Constant temperature heat transfer probe (Hsu *et al.* 1963; Delhay 1968), Optical probe (Miller & Mitchie 1970; Hinata 1972) and the more commonly used resistivity probe (Neal 1963; Nassos 1963; Lackme 1965; Malnes 1966; Herringe & Davis 1974, 1976). The last method relies on the change of electrical resistance between two electrodes when one or both electrodes are surrounded by either phase and is used when the liquid phase is conducting. Bubble velocity can be measured by placing two probes in series in the flow and determining by correlation technique the most probable time delay between individual bubbles passing over both probes (Lackme 1967; Malnes 1966; Herringe & Davis 1976; Serizawa *et al.* 1975). Measurement of local void passage times also leads to the determination of bubble size.

Sanderväg (1971) gave an interpretation of void fluctuations which would lead to an estimate of the bubble diameter probability density function in steam–water flow, whilst Uga (1972) derived a relation to convert bubble chord lengths density function to those for diameter. Herringe (1973) related bubble size to other parameters such as the bubble flux. Park *et al.*

(1974) examined relationships between the point bubble frequency as detected by a probe, the total bubble frequency and the bubble flux density. The present work aims to determine the local distribution of such flow structure parameters as void fraction, bubble frequency and velocity, bubble size and the average velocity ratio between the gas and the liquid phases at characteristic locations along a venturi. Due to its relatively developed state and ability to give reliable results in studies of two-phase structure, particularly in higher speed flow which would be expected at the venturi contraction, the resistivity probe technique was used.

## 2. MEASURING TECHNIQUES AND EXPERIMENTAL EQUIPMENT

### 2.1 Void fluctuation measurements

Figure 1 shows the construction of a double needle probe. Each active sensor is a small uninsulated region of a needle tip and the stainless steel casing is used as a return electrode. The sharp needles chosen for the probe had an average tip diameter of  $12\ \mu\text{m}$  whilst the exposed sensing area had a diameter of about  $50\ \mu\text{m}$ . The resistance between the needle tip and the stainless steel casing indicates whether the probe tip is immersed in the air or water phase. The phase detection circuitry adopted was similar to that used by Herringe & Davis (1974, 1976).

The time average of the rectangular two-state signal of the first needle gives the local void fraction  $\alpha$  which is defined as

$$\alpha = \lim_{T \rightarrow \infty} \frac{1}{T} \int_0^T \delta(x, t) dt, \quad [1]$$

where  $\delta(x, t)$  is a function which indicates the presence of either gas or liquid at the probe tip, namely

$$\delta(x, t) \begin{cases} = 1 & \text{when probe tip is in the gas phase} \\ = 0 & \text{when probe tip is in the liquid phase.} \end{cases} \quad [2]$$

In practice  $\alpha$  is easily obtained from the cumulative probability distribution function of the

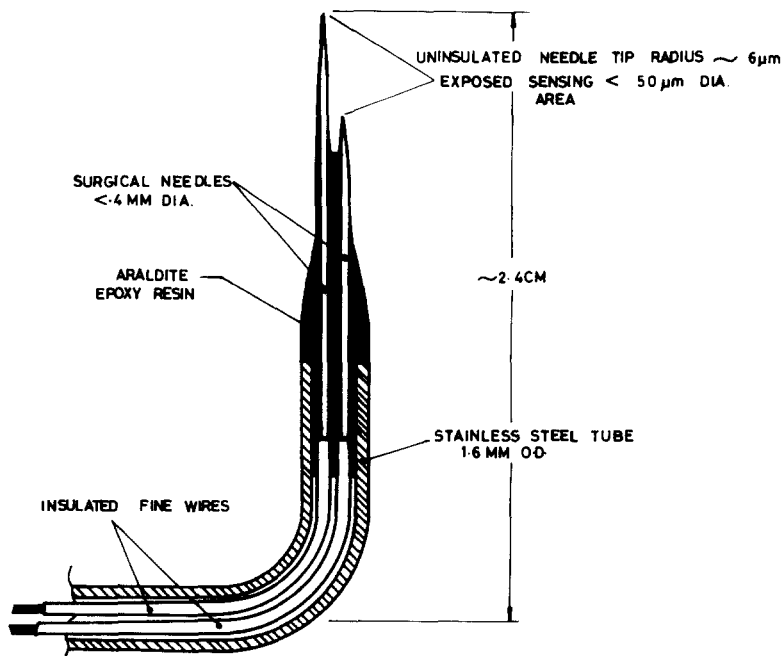


Figure 1. Construction of a double needle probe.

probe output signal. The cross-sectional average void fraction  $\{\alpha\}$  can then be obtained by integration of the local void fraction across the section.

The number of rectangular pulses can be averaged over a period of time to give the local bubble frequency. The output signal of the first needle is also correlated with that of the second needle where the cross-correlation function is defined by

$$R(x, \tau) = \lim_{T \rightarrow \infty} \frac{1}{T} \int_0^T \delta(x, t) \delta(x + X, t + \tau) dt \quad [3]$$

where  $X$  = axial separation distance of two probe tips;  $\tau$  = time delay.

The time delay  $\tau_0$  which gives maximum correlation is used to determine the mean velocity  $U_G$  of the bubbles ( $U_G = X/\tau_0$ ). Figure 2 shows some typical cross-correlograms recorded at the inlet of a venturi. Averaging the local gas phase velocity over the cross sectional area with weighting corresponding to local voidage yields the average gas velocity

$$\overline{U_G} = \frac{1}{\{\alpha\}A} \int_A \alpha U_G dA. \quad [4]$$

The measurement of void fraction and the cross-correlation of probe signals were performed using a Hewlett-Packard 3721A Correlator/Probability Analyser.

## 2.2 Determination of bubble size distributions

The probe output pulse widths are related to bubble chord lengths if the bubble velocity is known. Distribution functions of bubble diameters can then be obtained from a probability analysis of the pulse duration times through suitable transformation. The probability analysis of bubble size is based on the following main assumptions:

- (a) All bubbles are spherical;
- (b) Probe has equal probability of piercing any point on the projected frontal area of bubbles;
- (c) All bubbles travel in the same direction with the same average velocity  $U_G$ .

The first assumption would restrict the analysis to bubbly or dispersed flow situations because these are the cases for which bubbles may be reasonably assumed to be spherical. The second assumption essentially requires that the measuring point is sufficiently far from the wall in comparison with the bubble size. The last assumption will generally apply as long as the mean flow velocity is large compared with the local relative velocity and turbulent velocity. This last assumption is supported practically by the well defined sharply peaked correlations and transport times measured as shown in figure 2. To ensure a reliable detection of bubbles by the void probe it is also necessary to assume that the probe tip is infinitely small and there is no

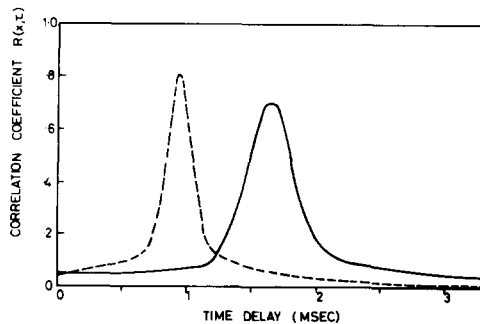


Figure 2. Normalized cross correlation functions recorded at inlet of venturi A1 (centre line position, 7.96 mm double needle streamwise separation). — Flow 4, 4.78 m/s velocity; ---- Flow 9, 8.53 m/s velocity.

deflection of bubbles by the probe. Generally this will be true if the probe tip is very small compared with the bubbles being detected as will be seen in the case in this investigation.

In the measurement, a bubble is generally detected by the probe along a chord length  $x$  which may vary from zero to the bubble diameter  $D$ . If  $g(x)$  is the probability density function of measured chord lengths of the bubbles and  $h(D)$  that of the detected bubble diameters, it can be shown (Herringe 1973; Herringe & Davis 1976) that

$$h(D) = \frac{1}{2} [g(x) - xg'(x)]. \quad [5]$$

The cumulative distribution function of  $h(D)$  is thus

$$H(D) = \int_0^x g(x) dx - \frac{1}{2} xg(x). \quad [6]$$

The mean diameter of all detected bubbles is given by

$$\bar{D} = \int_0^\infty Dh(D) dD \quad [7]$$

or

$$\bar{D} = 1.5 \int_0^\infty xg(x) dx \quad [8]$$

provided that  $x^2g(x)$  becomes zero when  $x$  approaches infinity. Hence

$$\bar{D} = 1.5 \bar{x} \quad [9]$$

where  $\bar{x}$  is the mean detected bubble chord length. The above relation can be used to calculate the mean detected bubble diameter without the need to determine its distribution function.

Herringe (1973) further introduced the probability density  $j(D)$  for diameters of all bubbles with centres passing through a unit area of the flow cross section, which may be more representative of the bubble size distribution than the function  $h(D)$  as the latter only deals with diameters of detected bubbles when there is a greater tendency for the probe to detect a large bubble than a small one at a given relative position for a given flux of bubbles per unit area. By denoting  $N$  as the total number of bubbles of all sizes whose centres pass through a unit area in a unit time and  $N_d$  the detected bubble frequency, it was shown that

$$j(D) = c \frac{h(D)}{D^2} \quad [10]$$

where

$$c = \frac{4N_d}{\pi N}. \quad [11]$$

From [10]

$$c = \left[ \int_0^\infty \frac{h(D) dD}{D^2} \right]^{-1}, \quad [12]$$

or by using [5]

$$c = 2 \left[ \lim_{x \rightarrow 0} \frac{g(x)}{x} \right]^{-1}. \quad [13]$$

The above equation may be used for calculating  $c$  if the bubble chord length distribution function  $g(x)$  is expressed by an analytical function of a suitable form. The ratio  $(N_d/N) =$

$(\pi c/4)$  represents the proportion of bubbles detected by the probe of all those whose centres pass through a unit area so that one would expect  $c$  to be relatively high where bubbles are large and low when there are only small bubbles.

Since the probability density function of the pulse widths cannot be obtained directly from the probe output signal, they are converted to very short duration pulses of proportionately variable heights and these pulses are then analyzed by an amplitude probability analyzer. The probability density function of the voltages of the pulse heights could then be converted back to the probability distribution of the original pulse duration times and hence detected bubble chord lengths  $g(x)$  (Thang 1976).

### 2.3 Venturi assemblies and experimental set-up

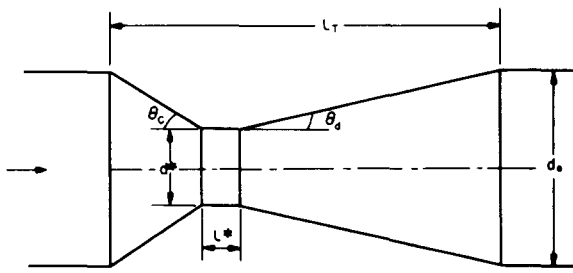
The test venturis were bored out of Perspex cylindrical blocks, the relevant geometrical features being given in table 1. The air-water mixture was produced by a multi-jet nozzle assembly in which the two phases were mixed in a contracting cone by turbulence generated by the jets. Under most conditions observed in this investigation a fairly uniform mixture was obtained (Herringe 1973; Herringe & Davis 1976). The mixture was introduced into a vertical clear pipe of 50.8 mm internal diameter upstream of the venturi. This settling pipe is 25 diameters long. The detailed work of Herringe & Davis (1976) showed that the flows from this mixer were very similar at this distance to those which occurred at much greater distances from various mixers and appeared to be independent of mixing method. On leaving the venturi, the flow passed through an additional main pipe 12 diameters long and was discharged through a return bend to the laboratory main sump.

## 3. VOIDAGE AND VELOCITY MEASUREMENTS

### 3.1 Visual observation of flow conditions

The flow conditions selected are given in table 2 and were found to give primarily bubble flow at the inlet to the venturi. Photographs of typical flow conditions are shown in figure 3. The mixture in the divergent passage appeared as an emulsion of very small bubbles, especially in high voidage and high velocity flows. Whilst it is possible to observe that the flow separates from the wall, the view of the central flow structure is often obscured by that of the flow closest to the wall. After the venturi exit, the bubbles started to grow rapidly in size along the tail pipe. There was an apparent reorganisation of the flow as it filled the pipe, the bubbles assuming an apparently spherical shape and showing a high degree of uniformity in size. These observations

Table 1. Geometrical details for venturi configurations



Venturis	$d^*$ (mm)	$d_0$ (mm)	$l^*$ (mm)	$l_T$ (mm)	$\theta_c$ (°)	$\theta_d$ (°)	$A_0/A^*$
A1	28.57	50.8	14.29	147.64	14.04	7.12	3.16
A4	28.57	50.8	14.29	69.85	45	14.04	3.16
B1	19.05	50.8	5.92	200.02	14.04	7.12	7.11
B4	19.05	50.8	5.92	88.90	45	14.04	7.11

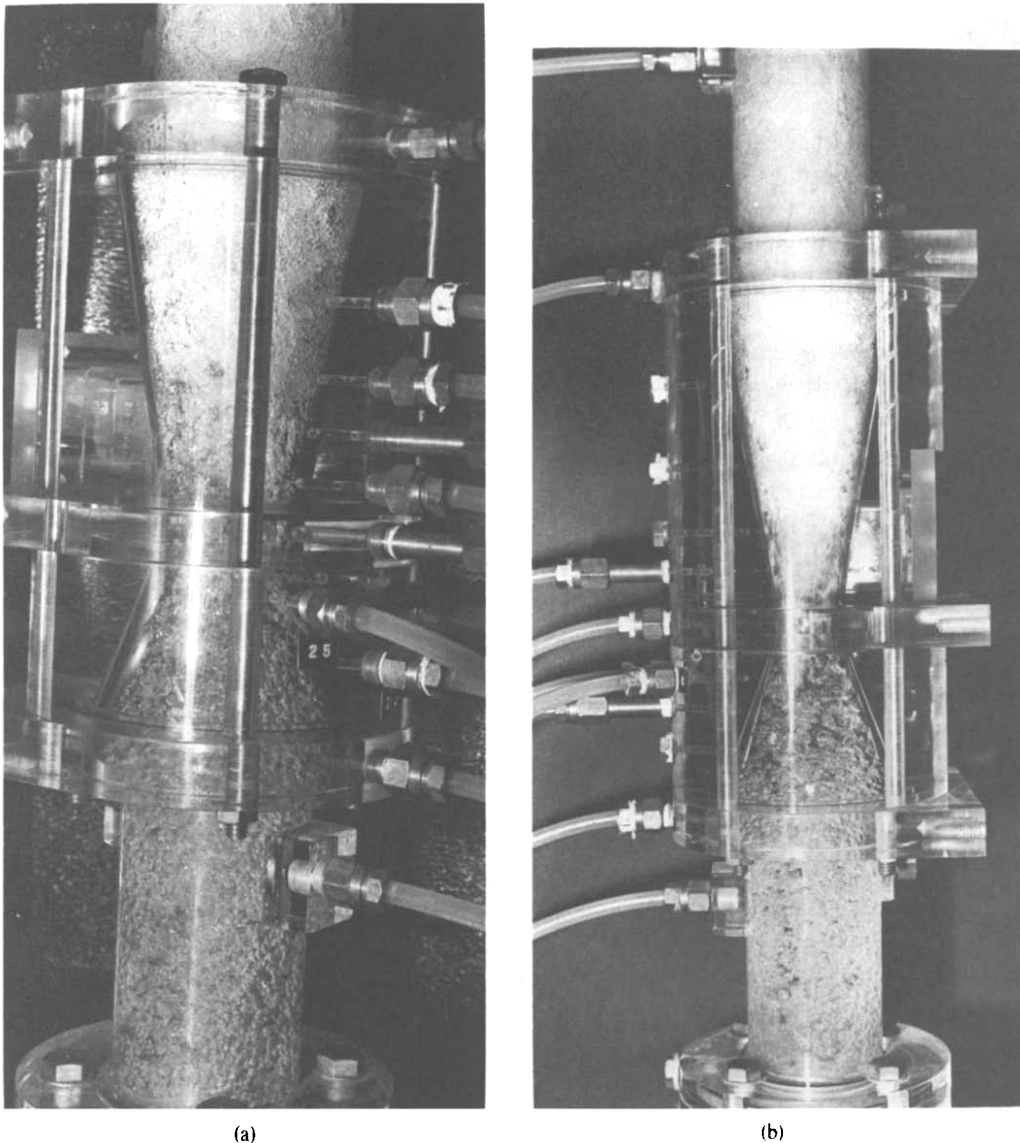


Figure 3. Flash photographs of flow in venturis. (a) Venturi A1, mean inlet conditions  $U_{m0} = 2.5$  m/s,  $\beta_0 = 0.21$ , (b) Venturi B1, mean inlet conditions  $U_{m0} = 2.0$  m/s,  $\beta_0 = 0.18$ .

show the marked change in the bubble structure between the convergent and divergent channels of the venturi.

### 3.2 Void and gas velocity profiles

The measured void profiles are shown alongside the measured velocity profiles in figure 4. As shown in table 2, flow conditions indicated by the same number for the two throat diameters are not the same due to different overall system constraints. At the inlet of venturi of series A (larger throat), an increase in the gas flow rate in flows having the same water flow rate appeared to cause more air to concentrate near the pipe centre. This was also found in flow conditions 1 and 3 in venturis of series B (smaller throat) whilst flow conditions 4 and 6 showed a concentration of air near the wall. Since the results of Herringe (1973) using the same type of mixer with comparable flow conditions also indicated profiles of similar shape which did not change even after 108 diameters in a straight pipe, it was concluded that this shape of the void profile was not caused by the venturi contraction but rather by the inlet flow rate conditions themselves. Further, measurement with a static pressure probe at the inlet showed that there

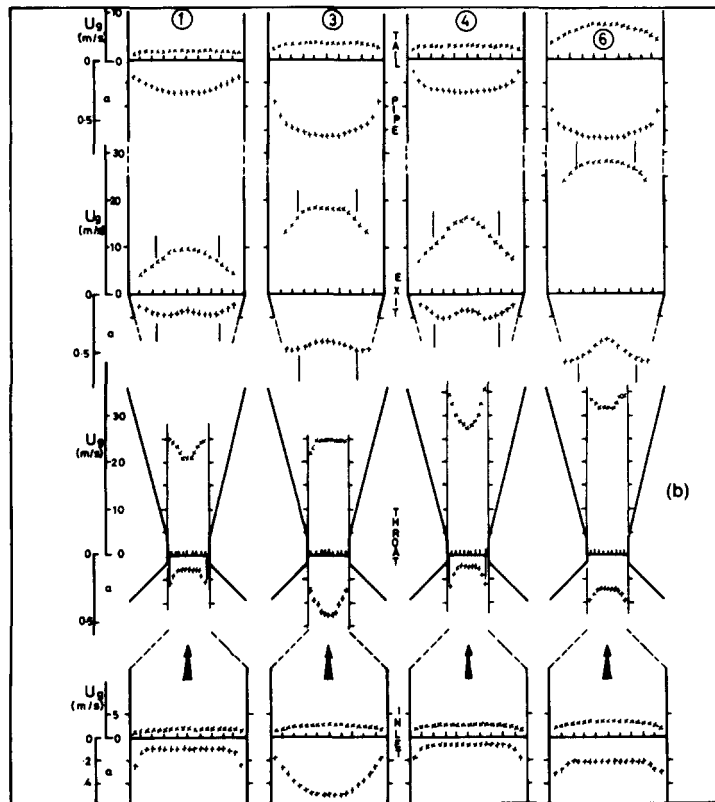
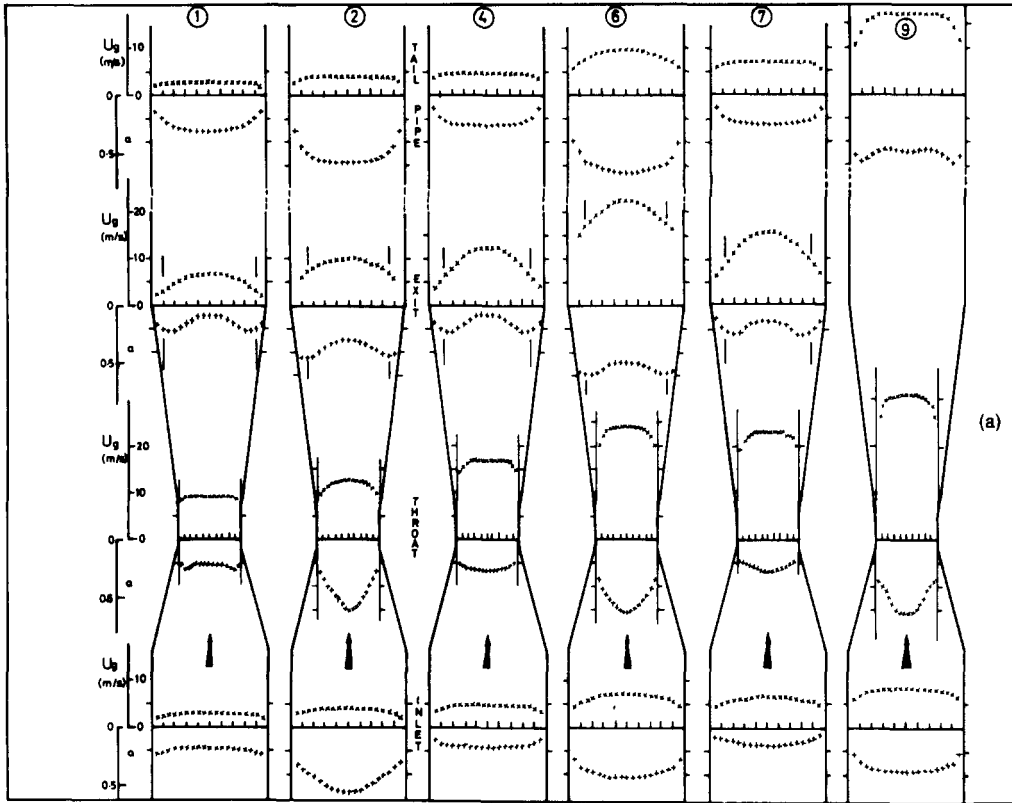


Figure 4. Void and velocity distributions in venturis (numbers denote flow conditions, table 2). (a) Venturi A1, (b) Venturi B4.

Table 2. Flow condition data

Venturi	Flow condition	$m_g \times 10^3$ (kg/s)	$m_l$ (kg/s)	$P_{inlet}$ (KPa)	$\beta^*$	$U_m^*$ (m/s)
A1	1	1.49	4.131	127.1	0.236	8.45
	3	4.07	4.131	136.6	0.455	11.84
	4	2.36	7.156	164.7	0.272	15.34
	6	11.36	7.156	235.9	0.545	24.54
	7	3.63	10.120	258.7	0.282	22.00
	9	22.97	10.120	441.9	0.506	31.97
B1	1	1.00	2.921	153.6	0.280	14.26
	3	4.04	2.921	201.8	0.544	22.54
	4	1.48	4.131	231.3	0.292	20.52
	6	5.54	4.131	333.1	0.448	26.32

$\beta^*$  = Gas volume fraction at the throat.

was no appreciable pressure gradient in the radial direction to indicate the influence of the venturi contraction in this region. It appeared then that void profiles with maxima near the wall were due to conditions of relatively low voidage and high pressure when there was less tendency for the air to migrate by turbulent mixing to the pipe centre.

At the throat of all venturis, the void profiles generally had similar shape to the corresponding ones at the inlet, suggesting that the mode of air distribution across the section did not experience any major reorganization as the flow moved through the convergent channel. However, local three-dimensional effects near the wall were observed in venturis A4 and B4 with a short convergent passage and a large inlet angle of 45°. In flow conditions 4 and 6 of venturi A4, the void profiles showed a sharp increase in gas concentration near the wall. This effect was due to the suction required to maintain the continuity of flow in the presence of a sharp convex corner. In venturi B4 (small throat) the sharp inlet wall of the throat section caused the flow to separate (vena contracta effect) in flow conditions 1 and 4 and the void profiles of these flow conditions were shown only to the flow boundary. Thus, it may be seen that the introduction of this increased local voidage close to the throat wall corresponds to conditions of higher flow mean density (i.e. lower average void fraction) and velocity when the suction pressure due to streamline curvature close to the wall is greater. It is noted that the lowest pressure measured on the wall in all flows was found to be fifteen times higher than the water vapour pressure and for this reason liquid phase cavitation was not expected to occur.

Void profiles at the exit showed that the flow changed its structure markedly as it emerged from the throat. From a fairly coarse bubbly mixture in the throat section, the flow at the exit appeared in the form of a jet-like diffusing transitional flow with bubbles being broken up into much smaller ones and a higher voidage in the outer radial regions. As the flow at the exit was shown to be separating from the wall, the estimated core flow size is indicated by two marking lines on the void profiles. The method of estimating this flow boundary is discussed in section 3.3.1. The main bulk of the flow momentum at the exit was concentrated in the middle of the jet, being transmitted by the faster moving, denser low voidage mixture at the centre of the exit section. Petrick (1958) in his measurements of void distribution using the gamma-ray attenuation technique in the flow following an abrupt expansion in a two-dimensional channel reported mean void profiles of similar shape which he termed "double annular". All void profiles at exit showed a central minimum surrounded by an annulus of higher voidage mixture except those of the longer venturi with the smaller throat (B1) where the mixture remained more nearly homogeneous in regard to its distribution of local void fraction. Sharper passage divergence thus appears to induce the higher local voidage conditions in the outer flow annuli at exit either on account of the separation induced within the throat section or else due to the higher inertia of the liquid phase and its reduced response to the radial pressure gradients which must exist in order to curve the streamlines in the diffuser if the flow is to fill the exit section pipe. Also, if



the flow in the diffuser is separated from the wall it may be seen that there is, on the basis of the negligible inertia of the gas phase, a tendency for the near stagnant recirculating region around the flow core to contain the gas phase rather than the liquid, which will not reduce the high streamwise velocity imparted to it in the throat as readily.

The void profiles at the tailpipe station indicated that most flows have developed into a relatively homogeneous pattern at ten diameters from the exit. The change in shape of the void profiles between the exit and downstream suggested that the high turbulence level in the transitional flow had contributed significantly to the local mixing of the flow as it filled the pipe. An exception was flow condition 9 where the void profile showed a local minimum in the centre. This was because the tailpipe station was still inside the transition zone required to re-mix the low voidage jet core flow emanating from the venturi exit, a longer transitional region being observed in this high velocity condition with a sharper exit passage divergence. It may be noted that the inlet void distribution has little or no apparent relation to that observed in either the venturi exit or in the tailpipe. In effect the venturi and its tailpipe have acted to strongly homogenize the flow, and a much longer length of downstream pipe flow would be required before void profiles with local maxima near the wall would reappear as suggested by the results of Herringe & Davis (1976).

When measuring void profiles in a vertical pipe, Herringe (1973) showed that in a number of low void fraction flows ( $\{\alpha\} \leq 0.2$ ) the profile shape most commonly found displayed a local minimum at the centre of the pipe and this shape did not change as the flow developed between 8 and 108 diameters from a nozzle mixer. The above type of profile was also found at 108D using two other types of mixer with different air injection methods. Herringe & Davis (1976) thus suggested that the profile shape with a minimum in the tube centre might represent a stable mode of void distribution in bubbly flows following a sufficient settling length. In this work, using the same nozzle mixer as in Herringe's case, profiles at the tailpipe section all tended toward a regular pattern with a maximum in the pipe centre. It thus appears that the absence of maxima near the wall in the void profiles downstream of the exit was due to the stronger turbulent mixing in the flows in conditions of generally higher velocity and voidage. In this case a void profile with a local minimum at the pipe centre when appearing at the inlet is not persistent in the flow, and the profile with a maximum in the tube centre may in fact characterize a stable and persistent mode of flow downstream of a venturi following a sufficient settling distance.

The gas velocity profiles (figure 4) generally show a central maximum. Departure from this trend was caused by suction due to a sharp contraction in the throat inlet of the venturis. In venturi A4, the profiles of low voidage flow conditions 1 and 4 displayed velocity maxima near the wall to show the accelerating effect of suction near the convex corner on the velocity of the gas phase. The increased gas content in flow conditions 3 and 6 has reduced the suction effect, resulting in no depression of the velocity profiles in the centre. Venturi A1 with its more moderate angle of convergence also did not show these effects. The velocity results showed that there is no general correspondence in the shape of the void and gas velocity profiles, particularly at the throat and the exit. The flows which developed locally high velocity near the wall in the throat were also found to exhibit a larger decrease of velocity with radius at the venturi exit. This is most likely due to the stronger separation of the flow associated with the higher suction voidage and velocity near the throat wall.

### 3.3 Accuracy of voidage and gas velocity measurements

3.3.1 *Flow separation at the exit.* In measuring at the inlet and throat stations, correlograms obtained from the double probe displayed fairly distinct peaks at measuring points across the section (e.g. figure 2). These clearly defined peaks, however, were not always found in the flow at the exit near the wall where the flow appeared to separate and create a recirculatory flow disturbance. When the probe was in the centre of the flow core at the exit, the correlogram

generally showed a distinct maximum. As it is moved toward the wall, this maximum decreased slightly as it was increasingly influenced by the separation region. When the probe went beyond the core flow boundary into the separated flow region, the correlogram maximum was observed to drop sharply. By observing the peak of the correlogram an estimate of the flow boundary could be made when the maximum was decreasing to a degree where the time delay could not be located within reasonable accuracy. Some typical correlograms of the flows at the exit of venturis A1 are shown in figure 5. The correlogram at the pipe centre is contrasted with that close to the separation boundary with the time scale for the latter increased ten times. Although the turbulent nature of the flow prevented the boundary of the flow core from being sharply defined, the fairly approximate method of determining the flow core diameter by the nature of the cross-correlation signals was adopted to enable the defining of an effective mean value for the void fraction and gas velocity from the respective profiles. The uncertainty in estimating the core size was smaller in flows with low void fraction (flow conditions 1, 4 and 7) where the core radius was estimated to within  $\pm 1.3$  mm or  $\pm 5\%$  of the pipe radius whilst for higher voidage flows (flow conditions 3 and 6), the accuracy was  $\pm 10\%$  of the pipe radius.

**3.3.2 Accuracy of voidage measurements.** In measuring void distribution with the probe, it is expected that the probe will cause disturbance to the flow. This disturbance gives rise to two separate effects: the deflection of bubbles from the front needle in a double probe which results in low readings for the void content and the interference of the first needle on the flow which will eventually be detected by the second needle.

It was difficult to estimate accurately the minimum size of the bubble that can be pierced successfully by the probe, especially when the sensing tip area was very small ( $6 \mu\text{m}$  tip radius for the probe used in this work). For a given probe having a sensing tip of a certain size, the minimum bubble size might also vary with conditions of the flow, particularly its velocity. Lacroart & Porte (1971) used an electrical impedance probe for measurement in flows with gas velocities greater than 10 m/s and suggested that the minimum bubble size could be assumed to be ten times

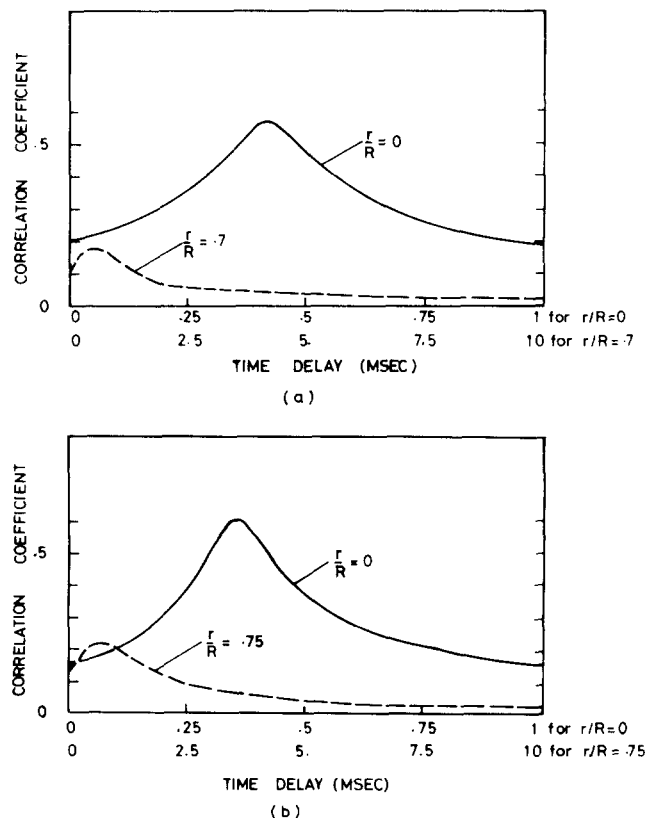


Figure 5. Correlation measurements at exit section of venturi A1, (a) Flow condition 3, (b) Flow condition 4.

the diameter of the sensing element. Other authors reported lower ratios between minimum bubble size and the size of the probe sensing element. Miller & Mitchie (1970) for example reported that an optical probe with a sensing element of diameter 0.3 mm could detect a bubble 0.5 mm in diameter at a superficial liquid velocity of 3 m/s. In the present work, it is reasonable to expect that for void probes with a sharp tip in flows with reasonably high velocity, bubble deflection would be contributing only small errors as will be subsequently demonstrated. This will be seen further when measured bubble size distributions are discussed (section 4). Other small errors in indicated void fraction were introduced by selection of the operating points of the Schmidt trigger circuit (Herringe & Davis 1976). A scaling was applied to correct the measured void fractions (section 3.3.3).

The second effect of disturbance, namely the interference of the first probe on the flow downstream in correlation measurements was also difficult to assess. In general, however, the missing of bubbles by either probe only affects the correlation coefficient and not the time delay at which maximum correlation occurred. The cross-correlation based on the response signals of both probes should thus provide reliable gas velocity results.

**3.3.3 Correction of void fraction results.** The gas volume flow rate  $Q_{G_1}$  detected by the probe as defined by

$$Q_{G_1} = \int_A \alpha U_G dA \quad [14]$$

was compared with that calculated from the inlet gas flow rate and pressure measurements ( $Q_{G_2}$ ). The results showed that at the inlet and downstream of the exit, the errors in the gas volume flow rates in all four venturis are fairly small, being 3.3% and 6.7% respectively on the average. At the throat the gas volume flow rate  $Q_{G_1}$  measured by the probe are lower than  $Q_{G_2}$  by an average of 10%. Due to the fine bubble structure at the exit which caused difficulties in operating the probe,  $Q_{G_1}$  are higher than the metered values  $Q_{G_2}$  by an average of 54%. Since the gas velocity measurement can be made fairly reliably using the double needle probe, the error in the gas volume flow rate  $Q_{G_1}$  when compared with  $Q_{G_2}$  is due largely to that in the measurement of void fraction. Therefore the void fraction readings were adjusted by a factor  $C$  which would give a gas volume flow rate equal to that derived from pressure and flow rate measurements. For simplicity  $C$  is assumed to be a constant across the section and is given by

$$C = \frac{Q_{G_2}}{Q_{G_1}}. \quad [15]$$

The adjusted void fraction averaged over the scaled profile is thus

$$\{\alpha_a\} = C\{\alpha\}. \quad [16]$$

This adjusted average void fraction allows the correct determination of the velocity of the gas phase in relation to the liquid phase, as this velocity ratio is sensitive to any errors in measuring  $Q_{G_2}$ .

#### 3.4 Velocity ratios

It was shown by Zuber & Findlay (1965) that relative velocity is caused by the existence of non-uniform distributions of void fraction and mixture velocity across the section. The following equation can be derived for the velocity ratio:

$$S = \frac{\frac{1}{\{\alpha\}} - 1}{\frac{1}{\beta} - 1} \quad [17]$$

where  $\beta$  is the volumetric flow fraction of gas phase.

The velocity ratio results for the four venturis are shown in figure 6. These values are based on values of  $\{\alpha\}$  corrected to ensure  $Q_{G2} = Q_{G1}$ . The velocity ratios were fairly close to unity at the inlet, varying in the range from 0.99 to 1.15. There was a general tendency for the velocity ratio to increase with void fraction here. At the throat, for the same size, venturis with a larger angle of convergence (A4 and B4) had higher velocity ratios. This can be understood in terms of the wall suction effect in these venturis. The above effect was also responsible for a reduction in the velocity ratio for an increase in the gas flow rate. The results in venturis with a more moderate angle of convergence (A1 and B1) also showed that the velocity ratio was decreasing with increasing void fraction at the throat. This suggests that local acceleration of the liquid phase by the gas phase and good mixing played a dominant role in limiting the average relative velocity when more gas flow was introduced. At the exit section, velocity ratio generally increased as the flow emerged from the throat. The velocity ratio here was subject to uncertainty due to difficulties in operating the probe and definition of the core flow boundary. The calculated velocity ratio ranged in value from 1.08 to 1.69 and was found higher the more the flow separated from the wall at the exit section, which might be caused by an increase in the gas flow rate and/or a short divergent passage. For bubbly flow at the tailpipe section, however, the velocity ratios were slightly higher than unity, and in these cases, were comparable in magnitude with those at the inlet.

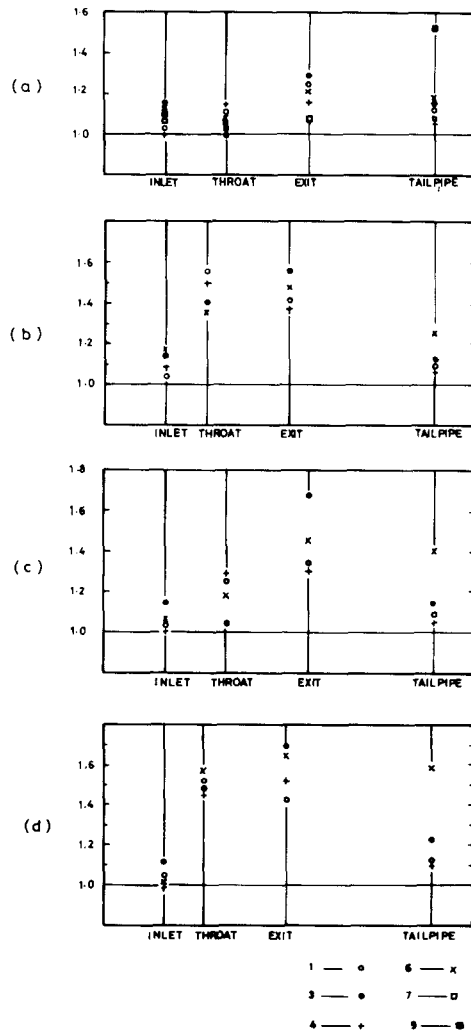


Figure 6. Variation of overall cross sectional velocity ratio. (a) Venturi A1, (b) Venturi A4, (c) Venturi B1, (d) Venturi B4. Flow conditions:  $\circ$ —1;  $\bullet$ —3; +—4;  $\times$ —6;  $\square$ —7;  $\blacksquare$ —9.

## 4. BUBBLE SIZE MEASUREMENTS

## 4.1 Profiles of mean bubble frequency and mean diameter

Equation [9] shows the relationship between the mean diameter of the detected bubbles and their mean chord length. Since a constant velocity  $U_G$  is assumed for all bubbles, the mean detected bubble diameter (denoted by  $b_m$  in this case) is related to the mean pulse duration time  $\bar{\tau}$  of the probe output signals by

$$b_m = 1.5 U_G \bar{\tau}. \quad [18]$$

The mean duration time  $\bar{\tau}$  can be readily determined from the local void fraction  $\alpha$  by

$$\bar{\tau} = \frac{\alpha}{N_d}, \quad [19]$$

where  $N_d$  is the number of pulses detected per unit time averaged over a sufficiently long period of time. Hence

$$b_m = \frac{1.5\alpha U_G}{N_d}. \quad [20]$$

As has been pointed out, the well-defined sharp peak of the correlation function (figure 2) indicates that the assumption of a single velocity for all bubbles is a reasonable approximation. Figure 7 shows the mean bubble frequency  $N_d$  and mean diameter  $b_m$  profiles in the venturis. Between the inlet and the throat for all flow conditions, an increase in the air flow rate, for flows having the same water flow rate, results in an increase in the mean bubble size and frequency in the pipe centre. Further increases in the air flow rate increase the inhomogeneity of the bubble structure and produce peaked mean diameter profiles with a maximum in the pipe centre, although profiles showing distinct maxima near the wall are evident in those flows when the void fraction is low. The nozzle mixer is observed to produce bubbles with relatively uniform size at the inlet in low voidage flows, mostly between 2 and 3.5 mm in diameter. The small increase in the bubble size between flow conditions 7 and 9 at the inlet of venturi A1 suggests that at high speeds, as the air flow rate is increased, the additional amount of air did not contribute a great deal to increases in the mean bubble size, but produced instead appreciable increases in the mean bubble frequency, a fact which may be attributed to the highly turbulent mixing action of the nozzle mixer.

An increase by a factor of four in mean bubble diameters at the throat pipe centre compared with those at the inlet was observed. This effect was also noted in the photographic records of Muir & Eichhorn (1963) for bubbles in flows with  $\beta^* < 0.3$  through the throat of a convergent-divergent nozzle. Table 3 gives the cross sectional averages,  $\{b_m\}$  of the mean detected bubble size and  $\{N_d\}$  of the bubble frequency. The results in all venturis suggest that the reduction in pressure at the throat is accompanied by an increase in bubble size whilst in between the throat and exit sections, a reduction in bubble size is always observed. The bubbles finally tend to values of mean diameters in the venturi tailpipe approx. 20% less than at the inlet, with a more uniform distribution of mean size across the pipe in all cases.

Comparison of the mean bubble size results of figure 7 with the void distributions of figure 4 shows that in general there is a close similarity between the two sets of profiles. That is, regions of high void fraction show an increased mean bubble size as might be expected. In the throat and exit regions it may be noted, however, that the bubble size distributions show relatively smaller peaks near the wall or central maxima than the void distributions. It appears therefore that these regions of high void fraction (especially in the smaller throats of venturis B1 and B4) are not accompanied by proportionate increases in mean bubble size, but by smaller increases

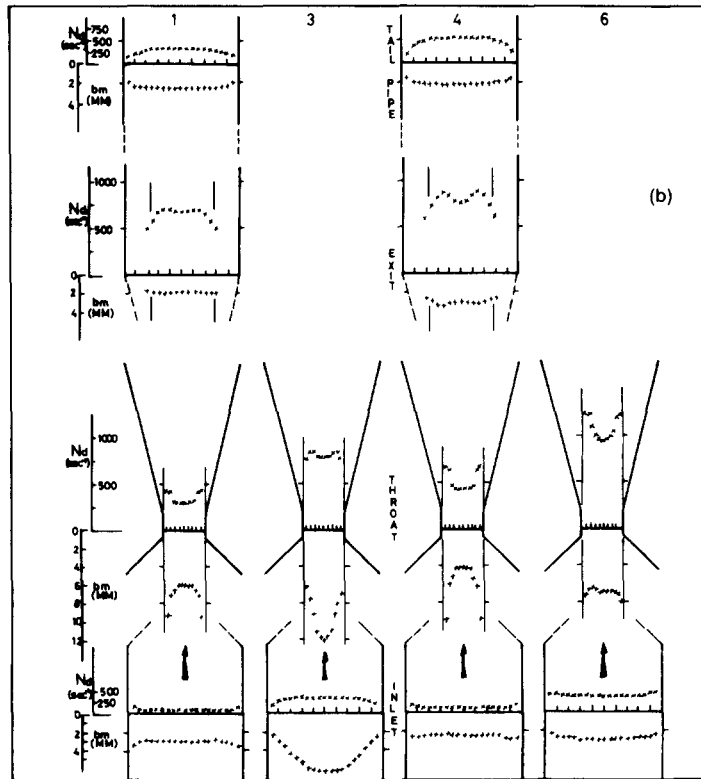
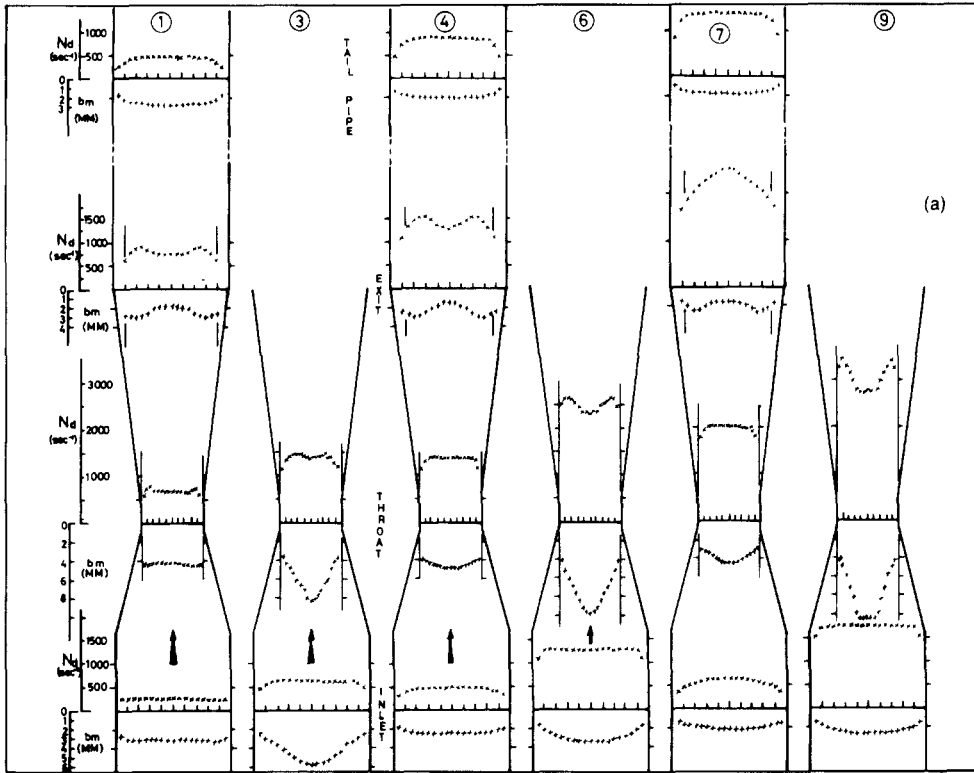


Figure 7. Profiles of detected bubble frequency  $N_d$  and mean diameter  $b_m$  (numbers denote flow conditions, Table 2). (a) Venturi A1, (b) Venturi B4.

Table 3. Cross sectional average values of mean bubble diameter  $\{b_m\}$  and bubble frequency  $\{N_d\}$ 

Venturi	Flow cond.	Inlet		Throat		Exit		Tailpipe	
		$\{N_d\}$ (s <sup>-1</sup> )	$\{b_m\}$ (mm)	$\{N_d\}$ (s <sup>-1</sup> )	$\{b_m\}$ (mm)	$\{N_d\}$ (s <sup>-1</sup> )	$\{b_m\}$ (mm)	$\{N_d\}$ (s <sup>-1</sup> )	$\{b_m\}$ (mm)
A1	1	243	2.85	637	4.07	809	2.71	357	2.25
	3	546	3.31	1244	4.60				
	4	381	2.08	1208	3.98	1442	2.68	685	1.66
	6	1160	2.34	2358	5.68				
	7	461	1.70	1800	3.27	2121	2.25	1108	1.45
A4	1	228	2.61	530	4.17	1186	1.98	368	1.99
	3	520	3.01	1095	4.01				
	4	326	1.97	1125	3.12	1653	2.75	788	1.38
	6	1097	2.08	2470	3.90				
B1	1	119	2.95	670	6.12	933	2.06	211	2.43
	3	303	3.65	1225	7.73				
	4	144	2.48	957	5.35	1342	2.27	350	2.19
	6	356	2.79	1700	6.75				
B4	1	106	2.85	750	7.26	1285	1.95	233	2.24
	3	252	3.75	1428	7.33				
	4	122	2.38	1137	6.38	1598	3.08	381	1.90
	6	349	2.52	2043	6.30				

in bubble size. Since the voidage depends upon the cube of bubble size such an effect appears physically reasonable. The question of whether overall fragmentation of gas voids occurs will be discussed in section 4.3.

#### 4.2 Bubble size distribution functions

Normalized probability density functions of detected bubble chord lengths  $g(x)$  for selected positions and flow conditions are shown in figure 8. The detected bubble diameter density function  $h(D)$  (converted from  $g(x)$  by [5]) is shown in figure 9. The bubbles are seen to grow in size and broaden considerably their size range at the throat as the gas phase expands. The high mean voidage flow conditions 3 and 6 generally showed a broader size distribution at the inlet and throat than flow conditions 1 and 4 with lower air content. In these latter flow conditions at the exit the flows contained very small bubbles formed by the breaking up of larger ones at the throat in a region of high turbulence due to flow separation (section 4.3). However, whilst the density functions of bubbles at the exit display their peaks at small diameters, they also indicate that an appreciable size range exists. The shift in the peaks of the probability density functions at the tailpipe section toward a larger bubble size than at the exit indicates an overall growth and homogenization of bubble size in the transitional flow lengths between the two sections. Reliable estimates for the mean detected bubble diameters can be calculated from either  $h(D)$  functions (denoted by  $\bar{D}$ , [7]) or from the void fraction and frequency measurements (denoted by  $b_m$ , [20]). Typical values are given in figure 9. These two estimates agree to within an average error of 5.4% for all cases.

The unit area flux diameter distribution  $j(D)$  in this work is generally subject to uncertainties which limit its applicability since  $j(D)$  requires the division by  $D^2$  of the detected diameter function  $h(D)$ . The available results show much narrower bubble size range and smaller mean diameters as compared with the corresponding detected diameter functions, particularly at the exit. The ratio  $(N_d/N)$ , which represents the proportion of bubbles detected by the probe of all those whose centres pass through a unit area, was found to vary between 0.3% and 14% for a unit area of 1 cm<sup>2</sup>.

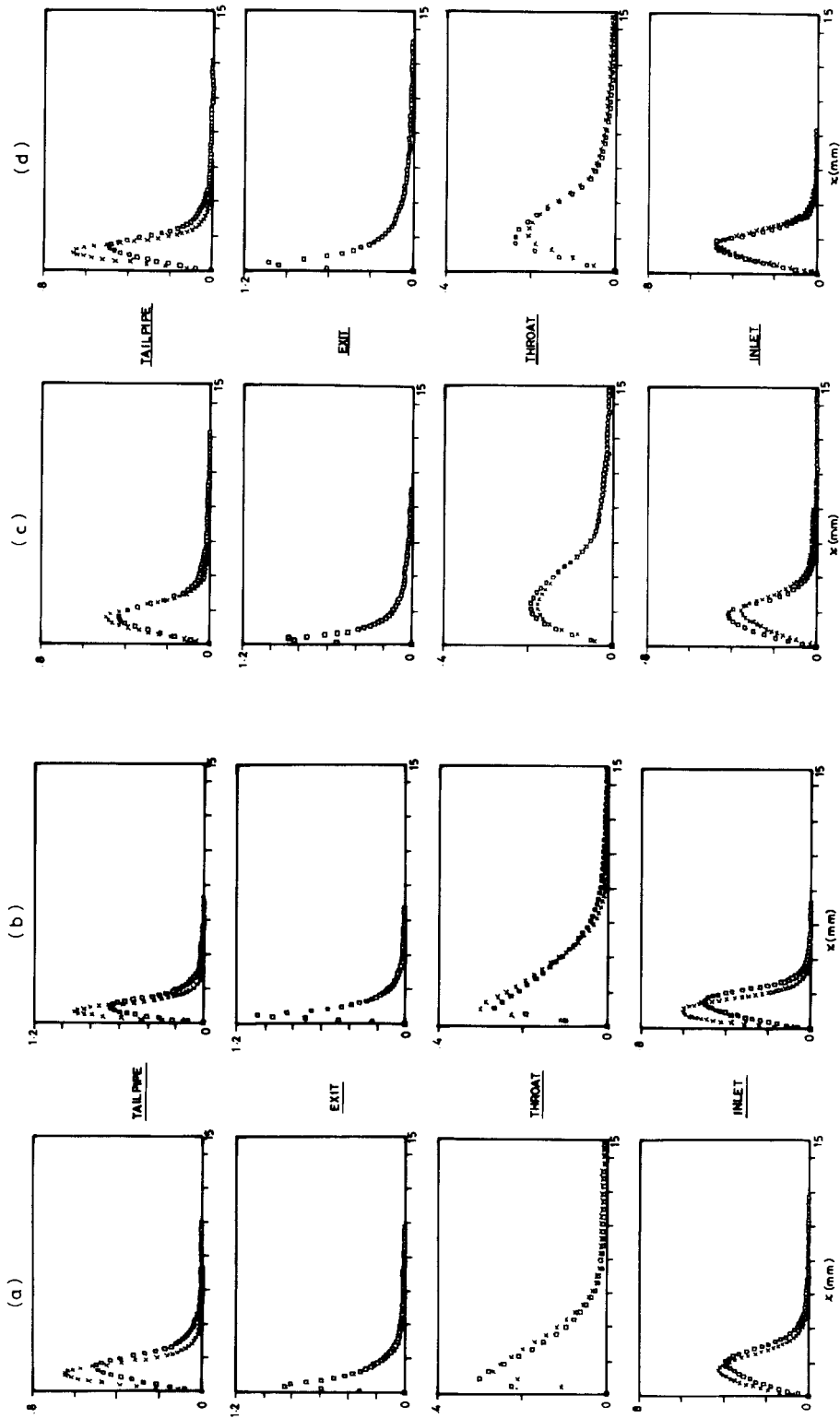


Figure 8. Probability density functions of detected bubble chord lengths  $g(x)$ .  $\square$ — $r/R = 0.0$   $\times$ — $r/R = 0.9$  or 0.777 at throat. (a) Venturi A1, flow 1; (b) Venturi A1, flow 1; (c) Venturi B1, flow 1; (d) Venturi B1, flow 4.



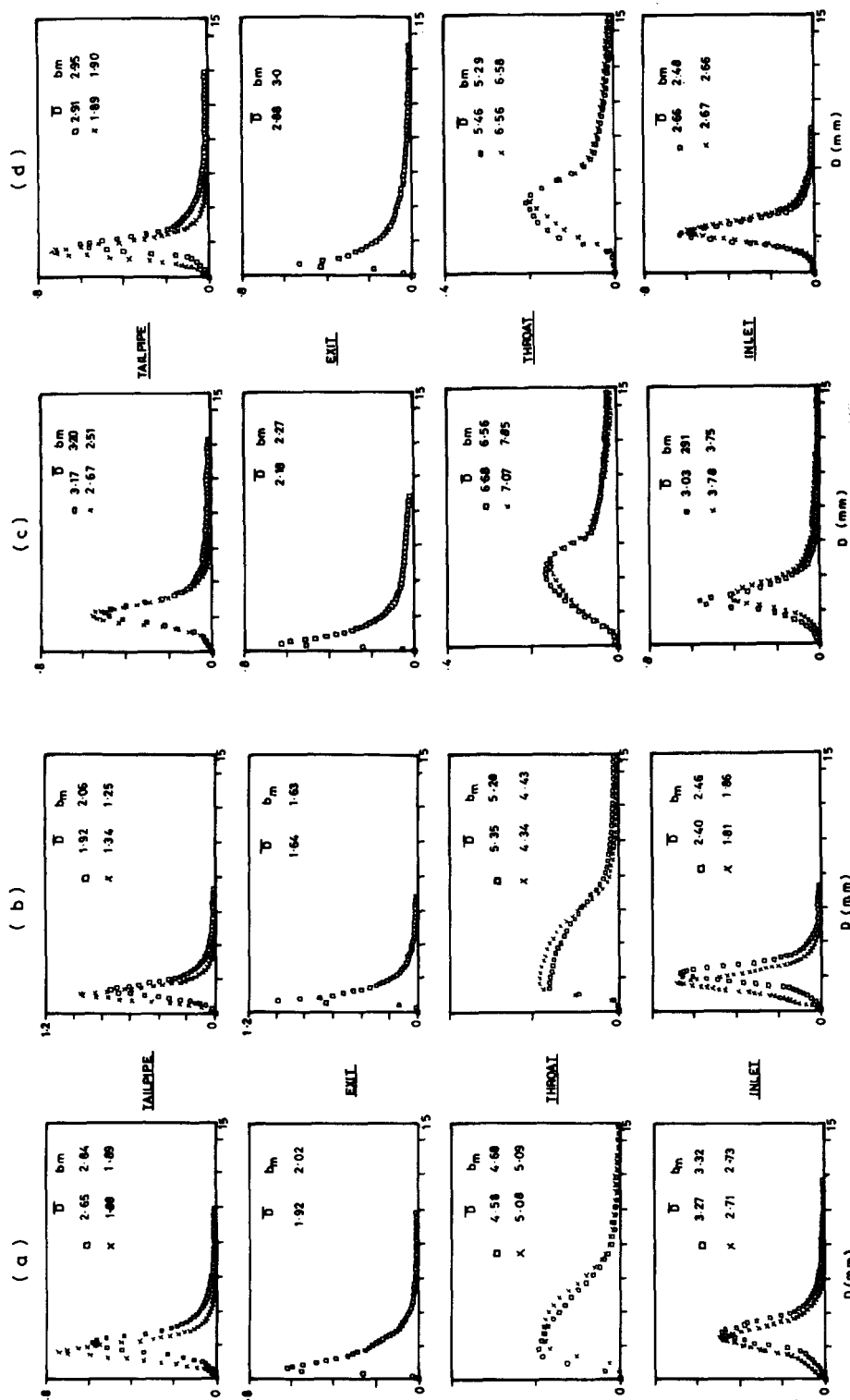


Figure 9. Probability density functions  $h(D)$  of detected bubble diameters.  $\square$ — $r/R = 0.0$   $\times$ — $r/R = 0.9$  or 0.777 at throat. (a) Venturi A1, flow 1; (b) Venturi A1, flow 4; (c) Venturi B1, flow 1; (d) Venturi B1, flow 4.

#### 4.3 Bubble coalescence and fragmentation

For the flow of a bubbly mixture across sections having cross sectional areas  $A_1$  and  $A_2$  and denoted by  $N_i$  the total number of bubbles passing through the cross section in a unit time, a condition for no overall tendency to coalescence or fragmentation of bubbles between the two sections is

$$N_{t1} = N_{t2}, \quad [21]$$

or alternatively

$$\{N_1\}A_1 = \{N_2\}A_2 \quad [22]$$

where  $N$  = local number of bubbles passing through a unit area in a unit time, and  $\{N\}$  = cross sectional average value of  $N$ . Thus

$$\{N_2\} = \{N_1\} \frac{A_1}{A_2}. \quad [23]$$

With regard to size, a given bubble is expected to change its volume in inverse proportion to the pressure in the absence of an overall coalescence or fragmentation. Thus denoting by  $\{b_m\}$  the cross sectional average bubble diameter, the latter will vary in inverse proportion to the cube root of pressure, namely

$$\{b_{m2}\} = \{b_{m1}\} \left( \frac{p_1}{p_2} \right)^{1/3}. \quad [24]$$

Equations [23] and [24] can be used to determine quantitatively whether the bubbles are subject to an overall coalescence or fragmentation between two sections of the flow. However, even if the results did indicate an absence of coalescence or fragmentation, this does not necessarily suggest that all bubbles pass through without some coalescence and fragmentation. Turbulence will lead to unsteady interactions which may break up the identity of individual gas elements as individual bubbles. Thus results which indicate no coalescence or fragmentation would show that such interactions average out to give no overall average trend for subdivision or amalgamation of gas elements. Further, in the absence of an overall coalescence or fragmentation, local values of bubble flux density  $N(r/R)$  at given positions determined by the same fractional radius  $r/R$  are related to the area ratio as in [23] if bubbles do not redistribute their centres in the radial direction between the two sections. Similarly, local mean bubble diameter  $b_m(r/R)$  are related to the pressure change as in [24] only if migration of bubbles across stream tubes is either absent or identical in extent for any size of bubble. In the general case, cross sectional average values of bubble flux density  $\{N\}$  and bubble diameter  $\{b_m\}$  can be used to test for the occurrence of bubble coalescence or fragmentation.

From [11] the bubble flux density  $N$  can be related to the point bubble frequency  $N_d$  by the constant  $c$  which is given by [12] assuming that bubbles do not radially redistribute their centres so that local values of  $N(r/R)$  at the same fractional radius  $r/R$  can be compared. In the larger throat venturi A1, the experimental bubble flux density at the centre of the exit section,  $N(0)$  in flow condition 4 was higher than the predicted value from [23] based on the corresponding throat condition by a factor of 15. In the smaller throat venturi B1, the value of  $N(0)$  for flow condition 1 at the exit section was also higher than the predicted value by a factor of up to 200. These results confirm that substantial fragmentation occurs downstream of the throat.

Cross sectional average bubble diameters can be compared with predicted values from [24]

as shown in tables 4 and 5. In all venturis, measured average bubble diameters at the throat are consistently larger than the predicted values based on pressure variation by an average of 70% in 18 flow conditions. The results thus indicate appreciable bubble coalescence in the inlet passage of the venturis. At the exit, the average bubble diameters predicted are larger than the measured values by an average of 210%, the difference being larger in the smaller throat venturis B1 and B4 which show an average difference of 280%. These results further confirm the existence of bubble fragmentation in the outlet passage. At the tailpipe section, the results in generally higher velocity flows show that bubble fragmentation may occur throughout the divergent passage and continue in the tailpipe. This is particularly relevant as the detected bubble diameters distribution functions  $h(D)$  measured at the exit section have indicated that the flow also contains some relatively large bubbles in an otherwise homogeneous froth of small bubbles, thus suggesting that the breaking up of bubbles downstream of the throat is not quite complete at the exit section. On the other hand, in relatively low velocity flows having a short transitional flow region bubbles may start to coalesce and form larger bubbles than expected at the tailpipe section as indicated by the results in flow condition 1 of venturis A4, B1 and B4. Overall it would appear that coalescence or fragmentation is not extensive in the flow downstream of the venturis' exit. Comparison of bubble sizes between the inlet and the tailpipe section shows that bubbles are fragmented as they travel through the complete venturi with bubbles at ten diameters downstream of the exit being smaller than expected from the pressure change by an average of 49%.

#### 5. CONCLUSIONS

The results indicate that following a sufficient settling length downstream of the venturis, all flows tended toward a well-mixed bubbly pattern with profiles of void fraction, bubble velocity and mean bubble size displaying a maximum in the tube centre. Variations of the inlet

Table 4. Comparison of measured average bubble diameters and predicted values assuming no coalescence or fragmentation—venturi A1

	Flow condition (mm)					
	1	3	4	6	7	9
Inlet (measured)	2.85	3.31	2.08	2.34	1.70	1.88
Throat (predicted from inlet)	3.04	3.57	2.57	2.81	2.28	2.32
Throat (measured)	4.07	4.60	3.98	5.67	3.27	5.85
Exit (predicted from throat)	3.99		3.70		3.31	
Exit (measured)	2.70		2.65		2.25	
Tailpipe (predicted from exit)	2.68		2.57		2.06	
Tailpipe (predicted from inlet)	2.98		2.32		2.12	
Tailpipe (measured)	2.25		1.66		1.45	

Table 5. Comparison of measured average bubble diameters and predicted values assuming no coalescence or fragmentation—Venturi B1

	Flow condition (mm)			
	1	3	4	6
Inlet (measured)	2.92	3.65	2.48	2.79
Throat (predicted from inlet)	3.53	4.33	3.29	3.43
Throat (measured)	6.12	7.73	5.35	6.75
Exit (predicted from throat)	5.72		5.31	
Exit (measured)	2.06		2.27	
Tailpipe (predicted from exit)	2.07		2.24	
Tailpipe (predicted from inlet)	3.31		3.22	
Tailpipe (measured)	2.43		2.19	

distributions of voidage were reflected at the venturi throat but not at positions further downstream. The overall reduction in pressure through the venturis was accompanied by an increase in mean fraction and gas velocity and a decrease in the mean bubble size. This increase in mean void fraction was accompanied by a substantial increase in the bubble number flux density, the bubbles coalescing in the convergent passage and fragmenting to very much smaller sizes primarily in the divergent passage. In venturis with sharp contractions, three-dimensional suction effects gave rise to an appreciable transverse pressure gradient at the throat section. This pressure gradient caused a localized increase in void fraction and acceleration of gas bubbles near the wall which contributed to a high overall relative velocity at the throat. This effect was observed to reduce with increasing void fraction, and thus shows a reverse trend to that where the velocity ratio generally increases with void fraction in the tailpipe section, this latter trend being more generally the case in gas-liquid flow in pipes.

## REFERENCES

- CAROFANO, G. C. & McMANUS, JR., H. N. 1969 An analytical and experimental study of the flow of air-water and steam-water mixtures in a converging-diverging nozzle. *Prog. Heat Mass Trans.* **2**, 395-417.
- DELHAYE, J. M. 1968 Measurement of the local void fraction in two-phase air-water flow with a hot-film anemometer. Rept. CEA-R-3465(E).
- HERRINGE, R. A. 1973 A study of the structures of gas-liquid mixture flows. Ph.D. Thesis, University of New South Wales, Australia.
- HERRINGE, R. A. & DAVIS, M. R. 1974 Detection of instantaneous phase changes in gas-liquid mixtures. *J. Phys. E. Scient. Instr.* **7**, 807-812.
- HERRINGE, R. A. & DAVIS, M. R. 1976 Structural development of gas-liquid mixture flows. *J. Fluid Mech.* **73**, 97-123.
- HINATA, S. 1972 A study on the measurement of the local void fraction by the optical fibre glass probe. First report, *Bull. J.S.M.E.* **15**, 1228-1235.
- HSU, Y. Y., SIMON, F. F. & GRAHAM, R. W. 1963 Application of hot-wire anemometry for two-phase flow measurements such as void fraction and slip velocity. A.S.M.E. Multiphase Flow Symposium, Philadelphia, 26-34.
- LACKME, C. 1965 Some statistical properties of two-phase flow in vertical tubes. Paper D2, Proc. Symposium on Two-Phase Flow, University of Exeter, England.
- LACKME, C. 1967 Structure et cinématique des écoulements diphasiques à bulles. Rept. CEA-R-3203.
- LECROART, H. & PORTE, R. 1971 Electrical probes for study of two-phase flow at high velocity. Int. Symposium on Two-phase Systems, Haifa, Israel.
- MALNES, D. 1966 Slip ratios and friction factors in the bubble flow regime in vertical tubes. Rept. KR-110, Kjeller Research Establishment, Norway.
- MILLER, N. & MITCHIE, R. E. 1970 Measurement of local voidage in liquid-gas two-phase flow systems using a universal probe. *J. Br. Nucl. Engng Soc.* **9**, 94-100.
- MUIR, J. H. & EICHHORN, R. 1963 Compressible flow of an air-water mixture through a vertical, two-dimensional, converging-diverging nozzle. Proc. 1963 Heat Transfer and Fluid Mechanics Institute, Stanford University Press, Stanford, 183-204.
- NASSOS, G. P. 1963 Development of an electrical resistivity probe for void fraction measurements in air-water flow. Rept. ANL-6738, Argonne National Laboratory.
- NASSOS, G. P. & BANKOFF, S. G. 1967 Local resistivity probe for study of point properties of gas-liquid flows. *Can J. Chem. Engng* **45**(5), 271-274.
- NEAL, L. G. 1963 Local parameters in concurrent mercury-nitrogen flow. Rept. ANL-6625, Argonne National Laboratory.
- PARK, W. H., LEE, N. G. & CAPES, C. E. 1974 Wall effects in point probe measurements of radial bubble distributions. *Chem. Engng Sci.* **29**, 339-344.

- PATRICK, M. 1958 Two-phase air-water flow phenomena. Rept. ANL-5787. Argonne National Laboratory, Illinois.
- SANDERVÅG, O. 1971 Thermal non-equilibrium and bubble size distribution in an upward stream-water flow. Rept. KR-144, Kjeller Research Establishment, Norway.
- SERIZAWA, A., KATAOKA, I. & MICHYOSHI, I. 1975 Turbulence structure of air-water bubbly flow. I. Measuring Techniques and II. Local Properties. *Int. J. Multiphase Flow* 2, 221-233 and 235-246.
- SMITH, R. V., COUSINS, L. B. & HEWITT, G. F. 1968 Two-phase two-component critical flow in a venturi. UKAEA Rept. AERE-R5736.
- THANG, N. T. 1976 A study of two-phase flow through venturis. Ph.D. Thesis, University of New South Wales, Australia.
- UGA, T. 1972 Determination of bubble size distribution in a BWR. *Nucl. Engng Design* 22, 252-261.
- VOGRIN, J. A., JR. 1963 An experimental investigation of two-phase, two-component flow in a horizontal converging-diverging nozzle. Rept. ANL-6754, Argonne National Laboratory.
- ZUBER, N. & FINDLAY, J. A. 1965 Average volumetric concentration in two-phase flow systems. *Trans. A.S.M.E., J. Heat Trans.* 87, 453-468.